

# Neutron Inelastic Scattering Processes as Background for Double-Beta Decay Experiments

D.-M. Mei,<sup>1,\*</sup> S.R. Elliott,<sup>1</sup> A. Hime,<sup>1</sup> V. Gehman,<sup>1,2</sup> and K. Kazkaz<sup>2,†</sup>

<sup>1</sup> *Los Alamos National Laboratory, Los Alamos, NM 87545*

<sup>2</sup> *Center for Experimental Nuclear Physics and Astrophysics, and  
Department of Physics, University of Washington, Seattle, WA 98195*

(Dated: August 11, 2013)

We investigate several  $\text{Pb}(n, n'\gamma)$  and  $\text{Ge}(n, n'\gamma)$  reactions. We measure  $\gamma$ -ray production from  $\text{Pb}(n, n'\gamma)$  reactions that can be a significant background for double-beta decay experiments which use lead as a massive inner shield. Particularly worrisome for Ge-based double-beta decay experiments are the 2041-keV and 3062-keV  $\gamma$  rays produced via  $\text{Pb}(n, n'\gamma)$ . The former is very close to the  $^{76}\text{Ge}$  double-beta decay endpoint energy and the latter has a double escape peak energy near the endpoint. We discuss the implications of these  $\gamma$  rays on past and future double-beta decay experiments and estimate the cross section to excite the level that produces the 3062-keV  $\gamma$  ray. Excitation  $\gamma$ -ray lines from  $\text{Ge}(n, n'\gamma)$  reactions are also observed. We consider the contribution of such backgrounds and their impact on the sensitivity of next-generation searches for neutrinoless double-beta decay using enriched germanium detectors.

PACS numbers: 23.40.-s, 25.40.Fq, 29.40.Wk

## I. INTRODUCTION

Neutrinoless double-beta decay plays a key role in understanding the neutrino's absolute mass scale and particle-antiparticle nature [1, 2, 3, 4]. If this nuclear decay process exists, one would observe a mono-energetic line originating from a material containing an isotope subject to this decay mode. One such isotope that may undergo this decay is  $^{76}\text{Ge}$ . Germanium-diode detectors fabricated from material enriched in  $^{76}\text{Ge}$  have established the best half-life limits and the most restrictive constraints on the effective Majorana mass for the neutrino [5, 6]. One analysis [7] of the data in Ref. [6] claims evidence for the decay with a half-life of  $1.2 \times 10^{25}$  y. Planned Ge-based double beta decay experiments [8, 9] will test this claim. Eventually, these future experiments target a sensitivity of  $> 10^{27}$  y or  $\sim 1$  event/ton-year to explore mass values near that indicated by the atmospheric neutrino oscillation results.

The key to these experiments lies in the ability to reduce intrinsic radioactive background to unprecedented levels and to adequately shield the detectors from external sources of radioactivity. Previous experiments' limiting backgrounds have been trace levels of natural decay chain isotopes within the detector and shielding components. The  $\gamma$ -ray emissions from these isotopes can deposit energy in the Ge detectors producing a continuum, which may overwhelm the potential neutrinoless double-beta-decay signal peak at 2039 keV. Great

progress has been made identifying the location and origin of this contamination, and future efforts will substantially reduce this contribution to the background. The background level goal of 1 event/ton-year, however, is an ambitious factor of  $\approx 400$  improvement over the currently best achieved background level [6]. If the efforts to reduce the natural decay chain isotopes are successful, previously unimportant components of the background must be understood and eliminated. The potential for neutron reactions to be one of these background components is the focus of this paper. The work of Mei and Hime[10] recognized that  $(n, n'\gamma)$  reactions will become important for ton-scale double-beta decay experiments. Specifically, we have studied neutron reactions in Pb and Ge, materials that play important roles in the Majorana [8] design. But since lead is used by numerous low-background experiments, the results will have wider utility.

This paper presents measurements and simulations of  $\text{Pb}(n, n'\gamma)$  and  $\text{Ge}(n, n'\gamma)$  reactions and estimates the resulting background for Ge-detector based, double-beta decay experiments for a given neutron flux. With these results, we then use the neutron flux, energy spectrum, angular distribution, multiplicity and lateral distributions determined in [10] to estimate the background in Ge detectors situated in underground laboratories. In Section II we describe the experiments, the data, and the simulations. In Sections III and IV we describe the analysis of these data. Section IV also discusses the important  $\text{Pb}(n, n'\gamma)$  production of  $\gamma$  rays at 2041 and 3062 keV. The former is dangerously near the 2039-keV Q-value for zero-neutrino double-beta decay in  $^{76}\text{Ge}$  and the latter can produce a double-escape peak line at 2040 keV. These dangerous processes for Ge-based double-beta decay experiments are discussed for the first time in this work. Section V determines an overall background model for our detector and the implications of this model for future experimental designs. It also considers the relevant

\*Permanent Address: The Department of Earth Science and Physics, University of South Dakota, Vermillion, South Dakota 57069

†Permanent Address: Lawrence Livermore National Laboratory, Livermore CA 94550

merits of Cu versus Pb as shielding materials, and the use of depth to mitigate these backgrounds is discussed. We also consider the possibility that the double-escape peak of the 3062-keV  $\gamma$  ray could contribute to the signal claimed in Ref. [7]. Finally, we summarize our conclusions in Section VI.

## II. THE MEASUREMENTS

We collected five data sets to explore the implications of  $(n, n'\gamma)$  for double-beta decay experiments. All measurements were done in our basement laboratory at Los Alamos National Laboratory. The laboratory building is at an atmospheric depth of 792 g/cm<sup>2</sup> and provides about 1 mwe concrete (77 g/cm<sup>2</sup>) overburden against cosmic ray muons.

Three data sets were taken with a CLOVER detector [11]. This detector is a set of 4 n-type, segmented germanium detectors. The four crystals have a total natural germanium mass of 3 kg and each crystal is segmented in half. The CLOVER detector and its operation in our laboratory were described in Ref. [12]. The remaining two measurements were done with a PopTop detector [13] set up in coincidence with a NaI detector. The PopTop is a 71.8-mm long by 64-mm diameter p-type Ge detector. Taking into account the central bore, the detector is 215 cm<sup>3</sup> or 1.14 kg. The NaI crystal is 15.25-cm long by 15.25-cm diameter and is directly connected to a photo-tube. All data were read out using a pair of X Ray Instrumentation Associates (XIA) [14] Digital Gamma Finder Four Channel (DGF4C) CAMAC modules. The CAMAC crate is connected to the PCI bus of a Dell Optiplex computer running Windows 2000. The system was controlled using the standard software supplied by XIA. This data acquisition software runs in the IGOR Pro environment [15] and produces binary data files that were read in and analyzed using the ROOT framework [16].

The data sets include:

1. A background run with the CLOVER
2. A Th-wire source run with the CLOVER
3. An AmBe source run with the CLOVER using two different geometries of moderator
4. An AmBe source run with the PopTop surrounded by lead
5. An AmBe source run with the PopTop surrounded by copper

In this section we describe the experiments and the data collected.

### A. The Experimental Configurations

The CLOVER was surrounded by 10 cm of lead shielding to reduce the signal from ambient radioactivity. Underneath and above the lead was 5 cm of 30%-loaded borated polyethylene to reduce thermal neutrons. The background run done in this configuration lasted 27.13 live-days. The configuration for the Th-source run was similar, but with some lead removed to expose the detector to the source. The Th source run had a live time of 1337 seconds.

The setup was modified somewhat from this background-run configuration for the measurements with the AmBe source. Fig. 1 shows the configuration for one of the AmBe measurements. For these data, the CLOVER was shielded on four sides with 10 cm of lead. The AmBe source, 30 mCi of <sup>241</sup>Am with a calibrated neutron yield of  $\approx 63,000$  Hz ( $\pm 0.7\%$ ), was on one side of the CLOVER with 5 cm of lead and a layer of pure polyethylene moderator (either 10 or 15 cm thick) between the source and detector. The data acquisition system is inactive during data transfer. Only the AmBe runs had a large enough event rate for the dead time to be appreciable. A 6.13-h live-time data run (57% live) was taken with 15 cm of moderator, and another 3.57-h live-time data (38% live) run was taken with 10 cm moderator (pictured). For the analysis presented below, the data from these two configurations were combined, and thus the AmBe-CLOVER data set contains 9.7 h of live time. The observed energy spectrum extended from  $\approx 10$ -3100 keV for these data sets.

During the analysis of the AmBe data, we observed a weak line at 3062 keV. This energy corresponds to a  $\gamma$ -ray transition in <sup>207</sup>Pb, and we therefore hypothesized that it was generated via Pb( $n, n'\gamma$ ). The double-escape-peak (DEP) energy (2040 keV) associated with this  $\gamma$  ray is very dangerous for <sup>76</sup>Ge neutrinoless double-beta decay experiments because it falls so close to the transition energy (2039 keV). Furthermore because the DEP is a single-site energy deposition, it cannot be distinguished from double-beta decay through event topology. This is in contrast to a full-energy  $\gamma$ -ray peak, which tends to consist of several interactions and therefore is a multiple-site deposition. (See [12] for a discussion of the use of event topology to reduce background in Ge detectors.)

The final two measurements were intended to study this 3062-keV line in the spectrum and demonstrate its origin. In both cases a PopTop Ge detector faced a 15.25 cm by 15.25 cm NaI detector for coincidence data. By sequentially placing a Pb and then a Cu absorber between an AmBe source and a PopTop Ge detector, we tested the hypothesis that the line was due to neutron interactions in Pb. By looking for an coincident energy deposit in the NaI detector, we could be assured the Ge detector signal originated from a neutron interaction in the sample. An energy deposit threshold in the NaI of greater than 200 keV was required for a coincidence. The PopTop was placed 27.3 cm from the NaI detector with the

source placed 20.3 cm (7 cm) from the Ge (NaI) detector. For the lead study, 5 cm of lead was placed directly between the Ge detector and the source. Additional lead, in the form of 5-cm-thick bricks was positioned around the 4 sides of the Ge detector to reduce room background. For the copper study, a 0.5-cm thick Cu tube was placed around the PopTop and a 5-cm Cu block was placed between the PopTop and the source. For this final run, all the lead was removed. For both of these sets of data, the observed spectra extended from  $\approx 125$  keV to  $\approx 9$  MeV. For the PopTop data, the Pb and Cu runs were of 19.12 h and 17.76 h live-time, respectively.

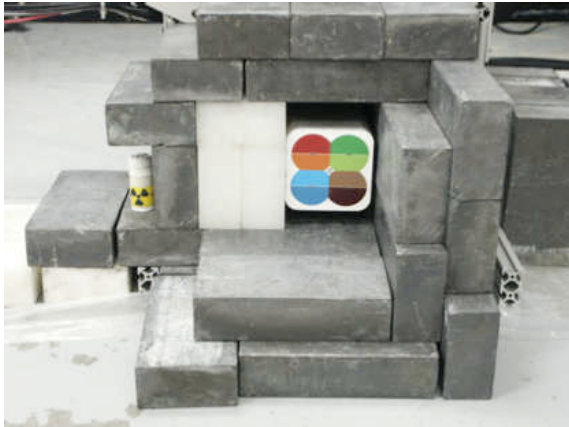


FIG. 1: The CLOVER detector as configured for the AmBe source run. The setup at the time of this photograph used 4" of polyethylene. One wall of the lead shield was removed only to clarify the relationship between the AmBe source, moderator, and the CLOVER.

## B. The Data sets

The crystals were individually calibrated, and the resulting spectra summed together to form a single histogram. The peaks within each of the 3 CLOVER data sets were identified and their intensities determined. If an event had 2 crystals that responded in coincidence, the histogram would have two entries. Therefore the spectra we analyzed and simulated included all single-crystal energy deposits. By not eliminating events that registered signals in more than 1 of the CLOVER Ge detectors, we maximized the event rate. The peak strengths were estimated by fitting a Gaussian shape to peaks and a flat background to the spectrum in the region near the peak. For the nuclear recoil lines, the peak shape was assumed to be a triangle and not Gaussian. In Table I the uncertainties derive from this fit. A summary of the peak strengths is given in Table I and the spectra themselves are shown in Fig. 2. The data sets were chosen to help decouple line blendings. Because the rates in all peaks and continua are much higher for the source-induced data than for the background, features in those

spectra are due to the sources and other contributions can be safely ignored. For example, the 2614.5-keV line can arise from either the decay of  $^{208}\text{Tl}$  or  $^{208}\text{Pb}(n, n'\gamma)$ . When exposed to a Th source, Tl decay dominates the spectrum, whereas when exposed to an AmBe source,  $(n, n'\gamma)$  dominates. Hence by normalizing the rate in this line to the rate in a pure neutron-induced transition (*e.g.* the 596-keV  $^{74}\text{Ge}(n, n'\gamma)$ ), we can determine the relative contribution of the two processes to the background spectrum. In fact, in the background data, both processes contribute to this line.

Some comments on our choices for line identification are in order. For an isotope such as  $^{72}\text{Ge}$  where a neutron capture leads to a stable nucleus, almost all  $(n, \gamma)$  lines could also be interpreted as  $(n, n'\gamma)$  lines in the resulting nucleus; in this case  $^{73}\text{Ge}$ . For isotopes within the detector however, such as the 53.5-keV  $^{72}\text{Ge}(n, \gamma)$  transition, the competing  $^{73}\text{Ge}(n, n'\gamma)$  line would be a sum of this  $\gamma$ -ray energy and the recoil nucleus energy. At these low energies where the recoil is a fair fraction of the  $\gamma$ -ray energy, the  $(n, n'\gamma)$  would simply contribute to the continuum and not be observed as a line. For the high energy cases, the blend of a mono-energetic  $\gamma$ -ray line and a  $(n, n'\gamma)$  process might be present.

For the calibration runs, our threshold was approximately 70 keV. Also note that we used a thorium wire as a calibration source. Since the wire is pure natural Th, we observe the Th X rays in that data. In contrast, the background run shows lines from the thorium chain as a contaminant, therefore those lines are absent.

In all spectra, there are a few lines we have not identified.

TABLE I: A summary of the observed lines in the various spectra taken with the CLOVER detector. Blank entries indicate that no significant peak feature above the continuum was found. Single and double escape peaks are labeled by SEP and DEP respectively. Line assignments for which we are unsure are indicated by a question mark. Line energies are taken from the Table of Isotopes [17].

Energy (keV)	Process	Count Rates		
		backgrnd (per hr)	Thorium (Hz)	CLOVER AmBe (Hz)
23.4	$^{70}\text{Ge}(n, \gamma)$			1.017(5)
46.5	$^{210}\text{Pb}$	112.75(42)		
53.2 } 53.5 }	$^{234}\text{U}$ } $^{72}\text{Ge}(n, \gamma)$ }	61.01(31)		2.079(8)
63.2	$^{234}\text{Th}$	93.02(38)		
67.7	$^{230}\text{Th}$	24.05(19)		0.591(4)
68.8	$^{72}\text{Ge}(n, \gamma)$			0.440(4)
72.80	Pb x-ray		10.5(1)	0.506(4)
74.97	Pb x-ray	663.5(1.0)	34.1(2)	1.703(7)
76.7	Unidentified		29.0(2)	
84.4 } 84.5 }	$^{228}\text{Th}$ } Pb x-ray }	115.28(42)	10.9(1)	0.930(5)
84.9	Pb x-ray			
87.2 } 87.4 }	Pb x-ray	55.65(29)	16.8(1)	0.262(3)
87.9				

Continued

TABLE I – continued

Energy (keV)	Process	Count Rates		
		backgrnd (per hr)	Thorium (Hz)	CLOVER AmBe (Hz)
89.9	Th x-ray		32.4(2)	
92.7	$^{234}\text{Th}$	171.38(51)		0.060(1)
93.4	Th x-ray		47.5(2)	
96.0	$^{115}\text{In}(n,\gamma)$ ?			0.166(2)
99.5	$^{228}\text{Ac}$	13.71(15)	3.0(1)	
105.3	Unidentified	8.99(12)		
104.8 } 105.6 }	Th x-ray		20.6(1)	
108.7	Th x-ray		7.6(1)	
109.9	$^{19}\text{F}(n,n'\gamma)$	43.00(26)		0.506(4)
129.1	$^{228}\text{Ac}$	12.91(14)	3.2(1)	
139.7	$^{74}\text{Ge}(n,\gamma)$	47.20(27)		2.339(8)
143.9	$^{230}\text{Th}$	20.03(18)		
154.0	$^{228}\text{Ac}$	7.69(11)	1.5(1)	
159.7	$^{77m}\text{Ge}$			0.114(2)
162.4	$^{115}\text{In}(n,\gamma)$	10.71(13)		1.073(6)
174.9	$^{70}\text{Ge}(n,\gamma)$	7.45(11)		0.763(5)
186.1 } 186.2 }	$^{226}\text{Ra}$ }	114.60(42)		0.323(3)
197.1 }	$^{115}\text{In}(n,\gamma)$ }			
198.4 }	$^{19}\text{F}(n,n'\gamma)$ }	81.04(35)		2.328(8)
	$^{71}\text{Ge}$ sum }			
199.2	$^{228}\text{Ac}$		0.66(2)	
202.6	$^{115}\text{In}(n,\gamma)$			0.061(1)
209.5	$^{228}\text{Ac}$	19.38(17)	10.9(1)	
215.5	$^{228}\text{Th}$	2.43(6)	0.92(3)	
238.6	$^{212}\text{Pb}$	295.77(67)	139.9(1)	0.105(2)
242.0	$^{214}\text{Pb}$	57.49(30)	9.2(1)	
247.1	$^{70}\text{Ge}(n,\gamma)$			0.070(1)
253.7	$^{74}\text{Ge}(n,\gamma)$	2.76(7)		0.410(3)
270.2	$^{228}\text{Ac}$	21.39(18)	9.1(1)	
273.0	$^{115}\text{In}(n,\gamma)$			0.055(1)
277.4	$^{208}\text{Tl}$			
	$\left\{ ^{208}\text{Pb}(n,n'\gamma) \right\}$	12.98(14)	5.4(1)	0.086(2)
284.6	Unidentified	2.79(7)		
288.1	$^{212}\text{Bi}$ ?		1.03(3)	
295.2	$^{214}\text{Pb}$	58.02(30)		
297.2 } 298.7 }	$^{72}\text{Ge}(n,\gamma)$ } $^{115}\text{In}(n,\gamma)$ }			0.068(1)
300.1	$^{212}\text{Pb}$	18.59(17)	9.7(1)	
306.2	$^{70}\text{Ge}(n,\gamma)$	1.12(4)		0.046(1)
321.4	$^{228}\text{Ac}$		0.67(2)	
326.0	$^{70,72}\text{Ge}(n,n'\gamma)$			0.487(4)
328.3	$^{228}\text{Ac}$	10.02(12)	8.2(1)	
332.9	$^{228}\text{Ac}$		1.14(3)	
335.5	$^{115}\text{In}(n,\gamma)$			0.028(1)
338.7	$^{228}\text{Ac}$	45.13(26)	31.5(2)	
351.9	$^{214}\text{Pb}$	95.11(38)		
354.1	Unidentified			0.043(1)
385.1	$^{115}\text{In}(n,\gamma)$			0.048(1)
391.3	$^{70}\text{Ge}(n,\gamma)$			0.053(1)
409.8	$^{228}\text{Ac}$	4.05(8)	4.3(1)	
416.9	$^{116m}\text{In}$	2.21(6)		0.359(3)
438.9	Unidentified	2.54(6)		
445.2	$^{74}\text{Ge}(n,\gamma)$			0.037(1)
452.3	$^{212}\text{Bi}$ ?		0.82(2)	
463.3	$^{228}\text{Ac}$	10.96(13)	9.2(1)	
474.0	$^{72}\text{Ge}(n,\gamma)$ ?	2.54(6)		

Continued

TABLE I – continued

Energy (keV)	Process	Count Rates		
		backgrnd (per hr)	Thorium (Hz)	CLOVER AmBe (Hz)
478.6	$^{228}\text{Ac}$		0.39(2)	
470-485	$\left\{ \begin{array}{l} ^{10}\text{B}(n,\alpha)^7\text{Li}^* \\ ^7\text{Li}^*(\gamma)^7\text{Li} \\ \text{Doppler} \\ \text{Broadened} \end{array} \right\}$			signf.
492.9	$^{73}\text{Ge}(n,\gamma)$			0.123(2)
499.9	$^{70}\text{Ge}(n,\gamma)$			0.453(4)
503.9	$^{228}\text{Ac}$		0.34(2)	
509.3	$^{228}\text{Ac}$			
510.7	$^{208}\text{Tl}$			
510.7	$^{208}\text{Pb}(n,n'\gamma)$	171.93(51)	16.8(1)	3.409(10)
510.9	Annih. $\gamma$			
516.2	$^{35}\text{Cl}(n,\gamma)$			0.160(2)
537.5	$^{206}\text{Pb}(n,n'\gamma)$	5.12(9)		0.158(2)
562.9 } 563.0 }	$^{228}\text{Ac}$ } $^{76}\text{Ge}(n,n'\gamma)$ }	12.83(14)	1.52(3)	0.244(3)
569.7	$^{207}\text{Pb}(n,n'\gamma)$	14.17(15)		0.422(4)
572.3	$^{228}\text{Ac}$		0.53(2)	
574.7	$^{74}\text{Ge}(n,\gamma)$			0.091(2)
583.1	$^{208}\text{Tl}$			
	$\left\{ ^{208}\text{Pb}(n,n'\gamma) \right\}$	71.64(33)	49.6(2)	0.256(3)
595.9	$\left\{ ^{74}\text{Ge}(n,n'\gamma) \right\}$	59.90(30)		1.869(7)
608.3	$^{73}\text{Ge}(n,\gamma)$			0.333(3)
609.2	$^{214}\text{Bi}$	60.11(30)		
629.6	$^{72}\text{Ge}(n,n'\gamma)$			0.078(2)
648.2	$^{115}\text{In}(n,\gamma)$			0.025(1)
657.2	$^{206}\text{Pb}(n,n'\gamma)$			0.047(1)
662.0	$^{137}\text{Cs}$	9.04(12)		
663.8	$^{206}\text{Pb}(n,n'\gamma)$			0.069(1)
669.0	$^{70}\text{Ge}(n,n'\gamma)$			0.030(1)
692.4	$^{72}\text{Ge}(n,n'e^-)$	87.70(37)		2.406(8)
701.0	$^{74}\text{Ge}(n,n'\gamma)$			0.082(2)
708.2	$^{70}\text{Ge}(n,\gamma)$			0.176(2)
727.3	$^{212}\text{Bi}$	15.72(16)	11.7(1)	
747.7	$^{70}\text{Ge}(n,\gamma)$			0.047(1)
755.3	$^{228}\text{Ac}$	2.19(6)	1.52(3)	
763.1	$^{208}\text{Tl}$		0.85(3)	
763.1	$^{208}\text{Pb}(n,n'\gamma)?$			0.032(1)
766.6	$^{224m}\text{Pa}$			
768.4	$^{214}\text{Bi}$	4.85(9)		
771.8	$^{228}\text{Ac}$		2.11(4)	
782.0	$^{228}\text{Ac}$	2.02(6)	0.67(2)	
785.5	$^{212}\text{Bi}$	4.19(8)	1.57(3)	
786.3	$^{35}\text{Cl}(n,\gamma)$			0.041(1)
786.8	$^{208}\text{Pb}(n,n'\gamma)$			
788.4	$^{35}\text{Cl}(n,\gamma)$			0.064(1)
788.7	$^{70}\text{Ge}(n,\gamma)$			
795.0	$^{228}\text{Ac}$	7.92(11)	6.1(1)	
798.0	$^{208}\text{Pb}(n,n'\gamma)$			0.023(1)
803.1	$^{206}\text{Pb}(n,n'\gamma)$	20.90(18)		0.850(5)
806.2	$^{214}\text{Bi}$	3.03(7)		
808.2	$^{70}\text{Ge}(n,\gamma)$			0.048(1)
818.6	$^{116m}\text{In}$			0.064(1)
824.9		1.03(4)		
830.4	$^{228}\text{Ac}$		0.70(2)	
834.1	$^{72}\text{Ge}(n,n'\gamma)$	45.15(26)		0.290(3)

Continued

TABLE I – continued

Energy (keV)	Process	Count Rates		
		backgrnd (per hr)	Thorium (Hz)	CLOVER AmBe (Hz)
835.6	$^{228}\text{Ac}$		2.30(4)	
840.4	$^{228}\text{Ac}$		1.19(3)	
843.8	$^{27}\text{Al}(n, n'\gamma)$	4.48(8)		0.112(2)
846.9	$^{76}\text{Ge}(n, n'\gamma)$			0.062(1)
860.4	$^{208}\text{Tl}$	8.64(12)	6.0(1)	0.090(2)
860.4	$^{208}\text{Pb}(n, n'\gamma)$			
865.0	Unidentified			
867.9	$^{73}\text{Ge}(n, \gamma)$	4.25(8)		0.466(4)
881.0	$^{206}\text{Pb}(n, n'\gamma)$	2.50(6)		0.151(2)
892.9	$^{212}\text{Bi}$		0.42(2)	
894.3	$^{72}\text{Ge}(n, n'\gamma)$			0.029(1)
897.8	$^{207}\text{Pb}(n, n'\gamma)$	6.28(10)		0.199(2)
904.1	$^{228}\text{Ac}$		0.94(3)	
911.2	$^{228}\text{Ac}$	48.86(27)	37.1(2)	
934.1	$^{214}\text{Bi}$	1.99(6)		
958.4	$^{228}\text{Ac}$		0.37(2)	
960.9	$^{74}\text{Ge}(n, n'\gamma)$			0.095(2)
964.4	$^{228}\text{Ac}$	11.22(13)	6.2(1)	
968.8	$^{228}\text{Ac}$	26.83(20)	21.6(1)	
981.0	$^{206,8}\text{Pb}(n, n'\gamma)$			0.035(1)
988.4	$^{228}\text{Ac}$	1.95(5)	0.20(1)	
993.7	$\left\{ \begin{array}{l} ^{74}\text{Ge}(n, n'\gamma) \\ ^{206}\text{Pb}(n, n'\gamma) \end{array} \right\}$			0.026(1)
995.1	$\left\{ \begin{array}{l} ^{74}\text{Ge}(n, n'\gamma) \\ ^{224m}\text{Pa} \end{array} \right\}$			0.034(1)
999.5	$^{74}\text{Ge}(n, n'\gamma)$	8.03(11)		
1001.5	$^{228}\text{Ac}$		0.17(1)	
1004.5	$^{27}\text{Al}(n, n'\gamma)$	7.46(11)		0.173(2)
1014.5	$^{228}\text{Ac}$		0.20(1)	
1033.1	$^{70}\text{Ge}(n, n'\gamma)$	16.89(16)		0.210(2)
1040.1				
1040.8				
1063.7	$^{207}\text{Pb}(n, n'\gamma)$	8.47(11)		0.145(2)
1065.0	$^{228}\text{Ac}$		0.47(2)	
1078.8	$^{212}\text{Bi}$	1.11(4)	0.62(2)	
1093.9	$^{208}\text{Tl}$ sum 511+583		0.90(3)	
1095	$\left\{ \begin{array}{l} ^{207}\text{Pb}(n, n'\gamma) \\ ^{70}\text{Ge}(n, \gamma) \\ ^{116m}\text{In} \end{array} \right\}$	7.81(11)		0.464(4)
1095.8	$^{70}\text{Ge}(n, \gamma)$			
1096.9	$^{116m}\text{In}$			
1101.3	$^{74}\text{Ge}(n, n'\gamma)$			0.123(2)
1105.6	$^{74}\text{Ge}(n, n'\gamma)$			0.019(1)
1110.4	$^{228}\text{Ac}$ sum		0.52(2)	
1120.6	$^{214}\text{Bi}$	11.70(13)		
1122.5	$^{228}\text{Ac}$ sum		0.26(1)	
1126	$\left\{ \begin{array}{l} ^{208}\text{Pb}(n, n'\gamma) \\ ^{72}\text{Ge}(n, n'\gamma) \end{array} \right\}$			0.022(1)
1131.6	$^{73}\text{Ge}(n, \gamma)?$	1.34(5)		0.034(1)
1139.4	$^{70}\text{Ge}(n, \gamma)$	1.34(5)		0.077(2)
1153.5	$^{228}\text{Ac}$		0.15(1)	
1155.2	$^{214}\text{Bi}$	1.08(4)		
1164.9	$\left\{ \begin{array}{l} ^{35}\text{Cl}(n, n'\gamma) \\ ^{72}\text{Ge}(n, n'\gamma) \end{array} \right\}$	0.49(3)		0.072(1)
1166.0	$\left\{ \begin{array}{l} ^{72}\text{Ge}(n, n'\gamma) \\ ^{60}\text{Co} \end{array} \right\}$			
1173.5	$^{60}\text{Co}$	13.67(14)		
1201.2	$\text{p}(n, \gamma)\text{d}$ DEP			0.415(3)
1204.2	$\left\{ \begin{array}{l} ^{73}\text{Ge}(n, \gamma) \\ ^{74}\text{Ge}(n, n'\gamma) \end{array} \right\}$	9.39(12)		0.163(2)
1226.7	$^{74}\text{Ge}(n, n'\gamma)$			0.017(1)
1238.4	$^{214}\text{Bi}$	5.22(9)		
1246.9	$^{228}\text{Ac}$		0.58(2)	

Continued

TABLE I – continued

Energy (keV)	Process	Count Rates		
		backgrnd (per hr)	Thorium (Hz)	CLOVER AmBe (Hz)
1261.0	$^{74}\text{Ge}(n, n'\gamma)$			0.019(1)
1281.0	$^{214}\text{Bi}$	0.74(3)		
1286.7	$^{228}\text{Ac}$ Blend		0.14(1)	
1293.5	$^{116m}\text{In}$	4.09(8)		0.462(4)
1298.8	$^{70}\text{Ge}(n, \gamma)$			0.087(2)
1332.5	$^{74}\text{Ge}(n, n'\gamma)$			0.018(1)
1332.5	$^{60}\text{Co}$	12.27(14)		
1344.5	$\left\{ \begin{array}{l} ^{74}\text{Ge}(n, \gamma) \\ ^{206}\text{Pb}(n, n'\gamma) \end{array} \right\}$	0.52(3)		0.017(1)
1345.9	$\left\{ \begin{array}{l} ^{70}\text{Ge}(n, \gamma) \\ ^{228}\text{Ac} \text{ sum} \end{array} \right\}$			
1347.7	$\left\{ \begin{array}{l} 964 + 409 \\ 911 + 463 \end{array} \right\}$			
1374.2	$^{214}\text{Bi}$	3.24(7)	0.28(1)	
1378.0	$^{70}\text{Ge}(n, \gamma)$			0.065(1)
1378.8	$^{206}\text{Pb}(n, n'\gamma)$			0.016(1)
1393.8	$^{214}\text{Bi}$	0.58(3)		
1401.5	$^{214}\text{Bi}$	1.84(5)		
1408.6	$^{73}\text{Ge}(n, n'\gamma)$			0.018(1)
1413.6	$^{228}\text{Ac}$		0.15(1)	
1431.1	$^{206}\text{Pb}(n, n'\gamma)$			0.020(1)
1433.5	$^{208}\text{Pb}(n, n'\gamma)$			0.017(1)
1436.9	$^{228}\text{Ac}$		0.80(2)	
1459.2	$^{40}\text{K}$	30.18(22)		0.066(1)
1461.0	$^{72}\text{Ge}(n, n'\gamma)$			0.114(2)
1463.9	$^{206}\text{Pb}(n, n'\gamma)$			0.032(1)
1466.8	$^{73}\text{Ge}(n, \gamma)$			0.047(1)
1471.6	$^{74}\text{Ge}(n, n'\gamma)$			0.025(1)
1489.2	$^{228}\text{Ac}$	0.73(3)	0.85(3)	
1496.2	$^{228}\text{Ac}$		0.42(2)	
1501.7	$^{116m}\text{In}$			0.069(1)
1508.9	$^{214}\text{Bi}$	1.95(3)		
1508.9	$^{212}\text{Bi}$		0.38(2)	
1512.7	$^{214}\text{Bi}$	0.54(3)		
1538	$^{228}\text{Ac}$		0.14(1)	
1557.1	$^{228}\text{Ac}$	0.68(3)	0.55(2)	
1580.8	$^{228}\text{Ac}$	6.06(10)	2.94(5)	
1588.3	$^{208}\text{Tl}$ DEP	7.24(11)	2.10(4)	0.107(2)
1592.5	$^{208}\text{Pb}$ DEP			
1592.5	$^{207}\text{Pb}(n, n'\gamma)$			
1593.0	$^{214}\text{Bi}$	0.38(2)		
1599.3	$\left\{ \begin{array}{l} ^{35}\text{Cl}(n, \gamma) \\ ^{74}\text{Ge}(n, n'\gamma) \end{array} \right\}$			0.018(1)
1601.1	$^{208}\text{Pb}(n, n'\gamma)?$			0.020(1)
1602.0	$^{212}\text{Bi}$	1.81(5)	1.32(3)	
1614.9	$^{228}\text{Ac}$		0.34(2)	
1620.5	$^{228}\text{Ac}$	1.82(5)	1.46(3)	
1625.0	$^{74}\text{Ge}(n, n'\gamma)$			0.021(1)
1630.7	$^{70}\text{Ge}(n, \gamma)$			0.016(1)
1631.5	$^{76}\text{Ge}(n, \gamma)$			
1632.0	$^{228}\text{Ac}$	0.43(3)	0.41(2)	
1634.0	$^{208}\text{Pb}(n, n'\gamma)$			0.026(1)
1638.3	$^{74,76}\text{Ge}(n, n'\gamma)$			
1640.4	$^{214}\text{Bi}$	0.36(2)		
1640	$^{228}\text{Ac}$		0.17(1)	
1661.3	$^{206}\text{Pb}(n, n'\gamma)?$			0.021(1)
1666.3	$^{206}\text{Pb}(n, n'\gamma)$	0.72(3)		0.041(1)
1699.5				
1704.5				

Continued

TABLE I – continued

Energy (keV)	Process	Count Rates		
		backgrnd (per hr)	Thorium (Hz)	CLOVER AmBe (Hz)
1710.9	$^{72}\text{Ge}(n, n'\gamma)$			0.327(3)
1712.2	$p(n, \gamma)d$ SEP			0.156(2)
1725.7	$^{207}\text{Pb}(n, n'\gamma)$			0.029(1)
1729.6	$^{214}\text{Bi}$	3.59(7)		
1764.7	$^{214}\text{Bi}$	11.68(13)		
1779.0	$\left. \begin{array}{l} ^{27}\text{Al}(n, \gamma)^{28}\text{Al} \\ ^{28}\text{Al} \Rightarrow ^{28}\text{Si} \end{array} \right\}$	2.13(6)		0.127(2)
1806.0	$^{212}\text{Bi}$		0.11(1)	
1844.5	$^{206}\text{Pb}(n, n'\gamma)$			0.044(1)
1846.9	$^{214}\text{Bi}$	2.26(6)		
1940.4	$^{74}\text{Ge}(n, n'\gamma)$			0.027(1)
1951.1	$^{35}\text{Cl}(n, \gamma)$			0.032(1)
1959.3	$^{35}\text{Cl}(n, \gamma)$			0.023(1)
2092.1	$^{206}\text{Pb}(n, n'\gamma)$			0.039(1)
2092.7	$^{207}\text{Pb}(n, n'\gamma)$			
2103.8	$\left\{ \begin{array}{l} ^{208}\text{Tl} \text{ SEP} \\ ^{208}\text{Pb} \text{ SEP} \end{array} \right\}$	5.21(9)	2.25(4)	0.090(2)
2112.1	$^{116m}\text{In}$			0.061(1)
2118.5	$^{214}\text{Bi}$	0.64(3)		
2204.0	$^{214}\text{Bi}$	3.73(8)		
2223.3	$p(n, \gamma)d$			5.813(13)
2390.5	$^{116m}\text{In}$			0.015(1)
2448.5	$^{214}\text{Bi}$	0.51(3)		
2614.5	$\left\{ \begin{array}{l} ^{208}\text{Tl} \\ ^{208}\text{Pb}(n, n'\gamma) \end{array} \right\}$	39.39(25)	16.3(1)	0.729(5)
2650.3	$^{206}\text{Pb}(n, n'\gamma)?$			0.011(1)
2686	sum $^{208}\text{Tl}?$		0.12(1)	
2892	sum $^{208}\text{Tl}$		0.08(1)	
3061.9	$^{207}\text{Pb}(n, n'\gamma)$			0.010(1)

### C. Neutron Spectra Simulation

We performed simulations of several geometries including:

1. A simulation of the cosmic-ray produced neutrons at our lab in Los Alamos and the response of the CLOVER detector to these neutrons within a 10-cm lead shield. This simulation is for comparison to our background data.
2. A simulation of the neutron flux induced on the CLOVER from the AmBe source with the 15 cm of intervening polyethylene.
3. A simulation of the neutron flux expected at 3200 mwe deep due to cosmic-ray  $\mu$  interactions in the surrounding rock and 30-cm lead shield and the response of the CLOVER to that flux

The first two of these simulations are to verify the code's predictive power. The third is to aid in understanding the utility of depth to avoid neutron-induced backgrounds.

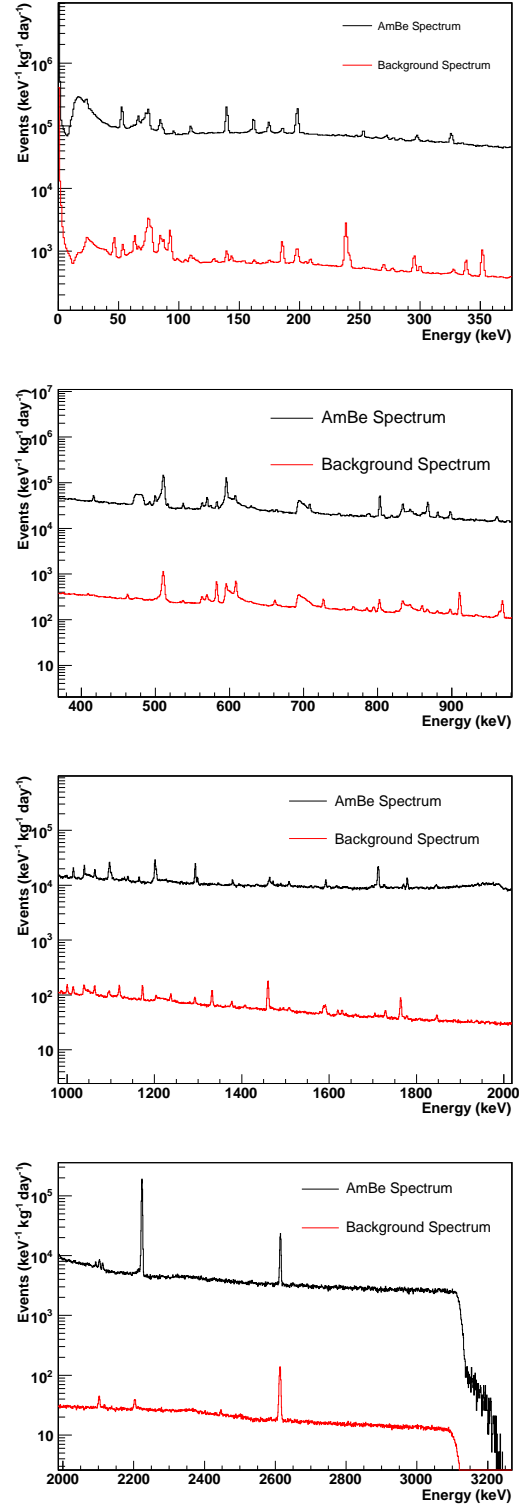


FIG. 2: The AmBe and background spectra taken with the CLOVER.

The simulation package GEANT3-GCALOR [18, 19] is described in detail in Ref. [10]. In general,  $(n, n')$  reactions leave the resultant nucleus in a highly ex-

cited state which subsequently decays via a  $\gamma$ -ray cascade to the ground state. In the simulation, inelastic scattering cross sections for excitation to a given level depends on the properties of the ground and excited states. These cross sections were calculated using in-house-written code based on Hauser-Feshbach [20] theory modified by Moldauer [21]. The validation of the Hauser-Feshbach theory has been the subject of several studies [22, 23, 24]. The simulated  $\gamma$ -ray flux arises from the relaxation of the initial excited-state distribution, which includes a large number of levels (60 states for  $^{208}\text{Pb}(n, n'\gamma)$  reactions, for example). The nuclear levels and their decay channels were provided by the ENSDF[25] database through the GEANT package. Note however, that the simulation did not predict every possible transition. In particular the important 2041-keV and 3062-keV emissions from Pb were not part of this simulation. This situation arises because the simulation packages only have  $(n, n')$  cross sections for the lowest lying excited states for most nuclei. It is set to zero for most other levels. The details of this simulation are described in detail in Ref. [10]. Here we study the effectiveness of the simulation to predict spectra resulting from  $(n, n'\gamma)$ .

The simulation was done by generating neutrons with the appropriate energy spectrum outside the lead shield and propagating them through the shield including secondary interactions that may add to the neutron flux and alter the energy spectrum. Fig. 3 shows a comparison between the data and the simulation for the CLOVER background run. Note only neutrons as primary particles were simulated for this comparison and the difference between the two spectra is due to the room's natural radioactivity and non-neutron  $\mu$ -induced processes. Here we excluded those processes from the simulation to emphasize the spectral shape, including lines, that are a direct result of neutron interactions. Table II shows a comparison of the simulation to the line production for the AmBe run. The comparison indicates that the simulated line strengths and continuum are accurate to approximately 30%.

### III. THE NEUTRON FLUX

In this section, we use the data to determine the neutron fluxes we observed during our various experimental configurations. We then compare our measured cosmic-ray induced flux with that predicted from past measurements and our simulation.

#### A. $\text{Ge}(n, n'\gamma)$ Analysis

Spectral lines that indicate neutron interactions in natural Ge detectors have been studied previously. See References [26, 27, 28, 29], for example. In particular, the *sawtooth*-shaped peaks due to  $^{72,74}\text{Ge}(n, n')$  at 693 keV and 596 keV respectively are clear indications of neu-

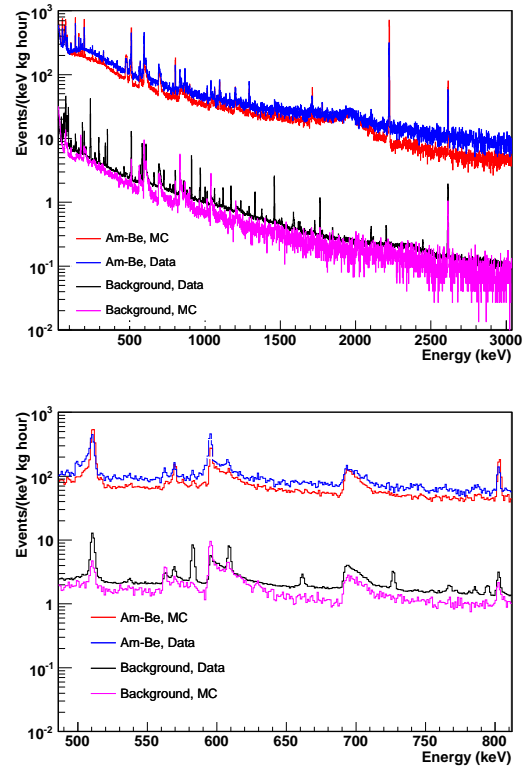


FIG. 3: Comparison of the measured and simulated AmBe spectra for the CLOVER detector surrounded by 10 cm lead and 15 cm of moderator. The upper plot shows the energy range between 10 - 3100 keV. The lower plot shows the range 470 - 830 KeV where the most significant  $(n, n'\gamma)$  lines can be seen. The simulated AmBe neutron spectrum was normalized to the AmBe source strength for 6.13-h live-time. The measured total neutron flux in the background spectrum (see Section III C) was used to normalize the simulated background spectrum. Note, only neutrons as primary particles were simulated for this comparison and the difference between the spectra is due to the room's natural radioactivity and non-neutron,  $\mu$ -induced processes.

trons and have been used to deduce neutron fluxes [30]. Operating Ge detectors in a low-background configuration, these lines can be used to help interpret the background components. Recent double-beta decay experiments [5, 6] have constructed their detectors from Ge enriched in isotope 76. Although an appreciable amount of  $^{74}\text{Ge}$  remained (14%),  $^{70,72,73}\text{Ge}$  are depleted. For such detectors, only lines originating in isotopes 74 and 76 are useful for neutron interaction analysis. As these experiments reach for lower background, neutron-induced backgrounds become a greater concern and the diagnostic tools more important.

Neutrons from  $(\alpha, n)$  and fission reactions have an energy spectrum with an average energy similar to the AmBe spectrum used in this study. Furthermore, the average energy of the AmBe neutrons is similar to that of the neutrons within the hadronic cosmic-ray flux imping-



TABLE II: A comparison of the simulated to measured rates in Hz for several lines produced by neutron interactions. The 2041-keV and 3062-keV lines are not predicted by the simulation. The accuracy of the simulation[10] was estimated to be approximately 30%.

Process	$\gamma$ -ray Energy	AmBe-CLOVER	
		Simulation	Measurement
$^{74}\text{Ge}(n, n'\gamma)$	596 keV	1.8	1.87
$^{74}\text{Ge}(n, n'\gamma)$	254 keV	0.36	0.41
$^{76}\text{Ge}(n, n'\gamma)$	2023 keV	$8.5 \times 10^{-4}$	below sensitivity
$^{206}\text{Pb}(n, n'\gamma)$	537 keV	0.15	0.16
$^{207}\text{Pb}(n, n'\gamma)$	898 keV	0.14	0.20
$^{206}\text{Pb}(n, n'\gamma)$	1706 keV	0.04	0.04
$^{206}\text{Pb}(n, n'\gamma)$	2041 keV	none	not seen
$^{207}\text{Pb}(n, n'\gamma)$	3062 keV	none	0.01

ing on our surface laboratory. Therefore the Ge-detector signatures indicating the presence of neutrons described above will be similar to those arising from neutrons originating from the rock walls of an underground laboratory. However, low-background experiments that use Ge detectors are typically deep underground and are shielded from environmental radioactivity by a thick shield. This shield, typically made of Pb, is then usually surrounded by a neutron moderator. This configuration is effective at greatly reducing the neutron flux originating from  $(\alpha, n)$  and fission reactions in the cavity walls of the underground laboratory. In contrast, neutrons originating from  $\mu$  interactions underground are much rarer and they have much higher energy. Therefore these  $\mu$ -induced neutrons can penetrate the shield more readily and become a major fraction of the neutrons impinging on the detector.

### B. The AmBe Neutron Flux

The estimate of the flux of neutrons with energies greater than 692 keV is given by [30, 31, 32]

$$\Phi_n = k \frac{I}{V}, \quad (1)$$

where  $I$  is the counts  $\text{s}^{-1}$  under the asymmetric 692-keV peak,  $V$  is the volume of the detector in  $\text{cm}^3$  ( $566 \text{ cm}^3$ ) and  $k$  is a parameter found by Ref. [30] to be  $900 \pm 150$  cm. For the 15-cm moderator data, this formula predicts a neutron flux of  $2.3/(\text{cm}^2 \text{ s})$  whereas our simulation predicts  $1.8/(\text{cm}^2 \text{ s})$ . This difference (20-30%) is comparable to the  $\sim 30\%$  difference found between the simulated and measured spectra (See Fig. 3) and is greater than the 17% uncertainty claimed by Ref. [30]. This reference used a  $^{252}\text{Cf}$  source, which has a different neutron energy spectrum than AmBe and perhaps that contributes to the difference. We use the 30% value as the estimate for the fast neutron flux uncertainty throughout.

For the Am-Be neutron source, the rate in the 692-keV peak is  $2.406 \pm 0.008$  Hz. This results in  $\Phi_n^{ambe} = 3.8 \pm 1.1 /(\text{cm}^2 \text{ s})$ . This rate is an average over the two moderator configurations. The neutron flux during the 10-cm moderator run is estimated to be about a factor 2.3 larger than for the 15-cm moderator run. For the PopTop-AmBe run on Pb for the raw data (in coincidence with the NaI detector), the effective flux was  $8.6 \pm 2.6/(\text{cm}^2 \text{ s})$  ( $0.26 \pm 0.08 /(\text{cm}^2 \text{ s})$ ).

### C. Cosmic-ray Induced Neutron Fluxes

In the background spectrum the rate in the 692-keV peak is  $87.7 \pm 0.4/\text{hr}$ . Using Eqn. (1) with  $I = (2.44 \pm 0.06) \times 10^{-2}$  Hz for the background spectrum, one obtains a fast neutron flux of  $\Phi_n^{back} = (3.9 \pm 1.2) \times 10^{-2} /(\text{cm}^2 \text{ s})$  at the detector in our surface laboratory.

Ref. [30] provides a similar formula to estimate the thermal neutron flux, which is accurate to approximately 30%. Using the intensity of the 139.68-keV  $\gamma$ -ray line of  $^{75m}\text{Ge}$ :

$$\Phi_{th} \left( \frac{n}{\text{cm}^2 \text{ s}} \right) = \frac{980 I_{139.68}}{(\epsilon_{139.68}^\gamma + 1.6) V}, \quad (2)$$

with

$$\epsilon_{139.68}^\gamma \simeq 1 - \frac{1 - e^{-V^{1/3}}}{V^{1/3}} \quad (3)$$

where  $I = 47.2 \pm 0.3 / \text{h} = 0.013$  Hz is the event rate in the peak of 139.68-keV line and  $V$  is the volume of the detector in  $\text{cm}^3$ . Using  $V = 566 \text{ cm}^3$  we obtain  $\Phi_{th}^{back} = (9.1 \pm 2.7) \times 10^{-3} /(\text{cm}^2 \text{ s})$ . We also measure the thermal neutron flux for the Am-Be neutron source,  $\Phi_{th}^{ambe} = 1.6 \pm 0.5 /(\text{cm}^2 \text{ s})$ .

Thus the total neutron flux incident on the Ge detector measured for the background run is approximately  $\Phi_{tot}^{back} = \Phi_n^{back} + \Phi_{th}^{back} = (4.8 \pm 0.7) \times 10^{-2} /(\text{cm}^2 \text{ s})$ .

### D. Neutron Flux as a Function of Depth

In our basement laboratory, there are 3 primary sources of environmental neutrons. The largest contribution comes from the hadronic cosmic ray flux. The next largest arises from  $\mu$  interactions in the  $77 \text{ g/cm}^2$  thick overhead concrete layer in the building. Finally there is the negligible contribution from  $(\alpha, n)$  and fission neutrons from natural radioactivity in the room. The atmospheric depth at the altitude of our laboratory is  $792 \text{ g/cm}^2$ . Including the concrete, the depth is  $869 \text{ g/cm}^2$ . Using the analysis of Ziegler [33, 34], the flux at our lab due to the hadronic flux can be estimated to be 3.0 times larger than that at sea level. The flux at sea level has been measured to be  $1.22 \times 10^{-2} /(\text{cm}^2 \text{ s})$  [35] resulting in a flux in our laboratory of  $3.7 \times 10^{-2} /(\text{cm}^2 \text{ s})$ . To estimate the additional neutron flux originating from



$\mu$  interactions in the concrete above our laboratory, we rely on our simulations of neutron generation and propagation. The simulation predicts  $1.4 \times 10^{-2} /(\text{cm}^2 \text{ s})$  ( $3.3 \times 10^{-2} /(\text{cm}^2 \text{ s})$ ) for the muon-induced (hadronic) neutron flux inside the lead shield for a total simulated neutron flux of  $4.7 \times 10^{-2} /(\text{cm}^2 \text{ s})$  in acceptable agreement with our measurement of  $4.8 \times 10^{-2} /(\text{cm}^2 \text{ s}) = 1.5 \times 10^6 /(\text{cm}^2 \text{ y})$ . The success of this simulation lends credence to the neutron flux estimate in the following sections.

The muon-induced neutron fluxes for several underground laboratories were calculated in Ref. [10]. Figure 4 shows the result of that calculation for the neutron flux at the rock-cavern boundary as a function of depth.

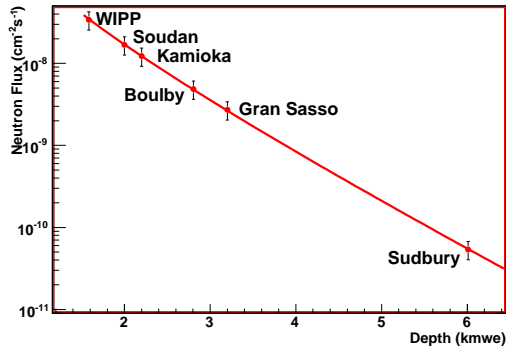


FIG. 4: The calculated neutron flux at the rock-cavern boundary as a function of depth. Back-scattered neutrons were excluded. The flux uncertainty estimate for each site is the quadrature sum of the muon flux and the neutron production rate uncertainties. The plot is obtained from Ref. [10].

The neutron flux onto the detector will be increased due to the neutron interactions with shield materials and neutron back-scattering from the cavity walls. For example, our simulations show that the fast neutron flux will increase by a factor of  $\approx 10$  by traversing a 30-cm lead layer. Also, neutrons will backscatter from the cavity walls and reflect back toward the experimental apparatus, effectively increasing the impinging neutron flux by a factor of 2-3 depending on the specific geometries of the detector and experimental hall. Therefore, it is important to account for these effects when estimating the neutron flux at the detector.

Muon-induced neutron production in different shielding materials and in the detector itself was also studied in Ref. [10]. For example, with 30 cm of lead surrounding a CLOVER-style detector at 3200 mwe, the total muon-induced neutron flux impinging on the detector was calculated to be  $\approx 8.6 \times 10^{-8} /(\text{cm}^2 \text{ s}) = 2.7 /(\text{cm}^2 \text{ y})$ . Some of the interactions resulting from these neutrons would be eliminated by a  $\mu$  veto. Assuming a veto efficiency of 90% for muons traversing this lead shield, the effective neutron flux is estimated to be  $2.0 \times 10^{-8} /(\text{cm}^2 \text{ s}) = 0.63 /(\text{cm}^2 \text{ y})$ . The energy spectrum of neutrons at the lead/detector boundary at 3200 mwe is shown in Fig. 5

and has an average value of 45 MeV.

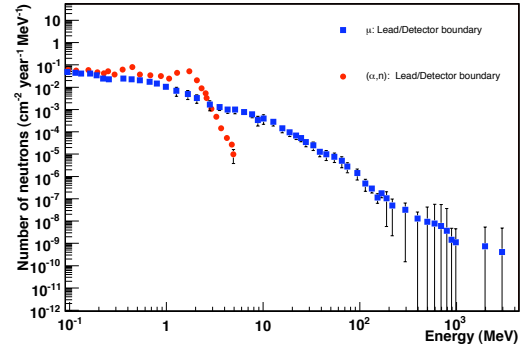


FIG. 5: The effective neutron flux onto the simulated detector described in the text at a depth of 3200 mwe. Shown are the neutron flux from two sources: (1) the effective neutron flux induced by muons that transverse the surrounding rock and shielding materials assuming a 90% muon-veto efficiency and (2) the neutron flux from  $(\alpha, n)$  reactions in the rock.

The average energy of the  $\mu$ -induced neutrons is 100-200 MeV and much higher than that of  $(\alpha, n)$  neutrons ( $\approx 5$  MeV). The simulated flux of the  $\mu$ -induced neutrons ( $2 \times 10^{-8} /(\text{cm}^2 \text{ s}) = 0.63 /(\text{cm}^2 \text{ y})$ ) inside the detector shield at a depth of 3200 mwe is a factor 2.4 greater than the simulated  $(\alpha, n)$  flux surviving the shield ( $0.85 \times 10^{-8} /(\text{cm}^2 \text{ s}) = 0.27 /(\text{cm}^2 \text{ y})$ ). The average energy of these  $(\alpha, n)$  originating neutrons is 3-5 MeV at the detector surface.

With this estimate of the neutron flux at depth and with our measurements of the Pb and Ge neutron-induced detector response, we can proceed to estimate these processes in underground Ge-detector experiments. There are effects in addition to the incident flux, however, that must be taken into account when extrapolating our surface laboratory results to different geometries and locations.

1. As the thickness of the Pb shield increases, additional secondary neutrons will be generated. Our simulation predicts that a factor  $k_{\text{shield}} = 2.16$  more neutrons will be produced by a 30-cm thick shield as compared to a 10-cm thick shield.
2. As the energy of the neutrons increases, the number of multiply scattered neutrons increases and therefore the number of interactions that might produce a  $\gamma$  ray increases. For the average energy of neutrons at our surface laboratory (at 3200 mwe), the average scattering length is  $\lambda_L = 7.1$  cm ( $\lambda_{UG} = 12.5$  cm).
3. Also as the energy increases, the number of states that can be excited in the target nucleus increases. In the shield at our surface laboratory (at 3200 m.w.e), the average neutron energy is 6.5 MeV (45 MeV).

All of these factors can be incorporated into a scaling formula derived from our simulation. The rate ( $R_{ROI}^{UG}$ ) of background near the region of interest (ROI) in an underground laboratory can be related to that measured in our surface laboratory ( $R_{ROI}^L$ ) as

$$R_{ROI}^{UG} = (1 + \frac{\lambda_{UG}}{\lambda_L}) k_{shield} ((\frac{E_n^{UG} - E_x}{E_n^L - E_x})^{0.8}) \frac{\Phi_n^{UG}}{\Phi_n^L} R_{ROI}^L, \quad (4)$$

where  $\Phi_n^L$  ( $\Phi_n^{UG}$ ) is the neutron flux in our surface laboratory (at 3200 mwe),  $E_n$  is the neutron energy and  $E_x$  is the excitation energy for a typical level. This formula reproduces our simulated results to within about 20%. Using the 2.6-MeV level in  $^{208}\text{Pb}$  as an example,  $R_{ROI}^{UG} \sim 1.7 \times 10^{-5} R_{ROI}^L$ .

#### IV. ANALYSIS

##### A. $\text{Pb}(n, n'\gamma)$ analysis

If fast neutrons are present, then one will also see  $\gamma$ -ray lines from  $\text{Pb}(n, n')$  interactions. In very low background configurations,  $\gamma$  rays from neutron-induced excitations in  $^{208}\text{Pb}$  and  $^{207}\text{Pb}$  can be masked by or confused for decays of  $^{208}\text{Tl}$  and  $^{207}\text{Bi}$  respectively. Therefore it is the stronger transitions in  $^{206}\text{Pb}$  (537.5, 1704.5 keV) that are most useful for determining if these processes are taking place. In  $^{207}\text{Pb}$  the relative strength of the 898-keV transition, compared to the 570- and 1064-keV transitions, is much stronger when it originates from  $^{207}\text{Pb}(n, n'\gamma)$  as opposed to  $^{207}\text{Bi}$   $\beta$  decay to  $^{207}\text{Pb}$ . Therefore this line can also be used as a tell-tale signature of neutron interactions.

Our data show indications of  $^{206,207,208}\text{Pb}(n, n'\gamma)$ . As noted earlier, the 2614-keV  $\gamma$  ray from  $^{208}\text{Pb}$  can originate from  $^{208}\text{Tl}$  decay or from  $^{208}\text{Pb}(n, n'\gamma)$ . The 692-keV peak arises only from neutron interactions on  $^{72}\text{Ge}$ . Since the Pb shielding was similar in both the background and AmBe runs, we can compare the ratio of the rate in the 2614-keV peak to that in the  $^{72}\text{Ge}(n, n'\gamma)$  692-keV peak in the two data sets to deduce the fraction of the 2614-keV in the background run that can be attributed to neutron interactions. This ratio in the Am-Be spectrum is 0.30 and that in the background spectrum is 0.45, and therefore, we conclude that  $\approx 67\%$  of the strength in the background run is due to neutron reactions and the remainder is due to  $^{208}\text{Tl}$  decay. Clearly, in our surface laboratory, environmental neutrons are a significant contributor to the observed signal.

Like neutron interactions on Ge, the line strengths from  $\text{Pb}(n, n'\gamma)$  change with neutron energy. The probability that a given energy level in Pb is excited depends on neutron energy. For example, Fig. 2 in Ref. [23] dramatically shows how the 898-keV line, that is well-separated from nearby lines and clearly visible at an average energy of  $\approx 14$  MeV, is partially obscured by a

near-continuum of lines when the average neutron energy is 100-200 MeV. Figure 6 shows a simulation of the production of the 692 and 2614-keV  $\gamma$  rays due to neutron interactions. This plot shows the strong energy dependence of the production rate, but also that the predicted ratio of the production rates of the  $^{208}\text{Pb}(n, n'\gamma)$  2614-keV and the  $^{72}\text{Ge}(n, n'\gamma)$  692-keV  $\gamma$  rays is rather insensitive to energy. For the average energy of the AmBe source (5.5 MeV), the predicted ratio is  $0.32 \pm 0.11$  and for the background-neutron average energy (6.5 MeV) the predicted ratio is  $0.37 \pm 0.13$ . Our measurement with the AmBe source results in a ratio of 0.30 in good agreement with these predictions. To scale these results to the underground situation requires an extrapolation of the production rate with respect to energy. Presently this extrapolation is done via simulation of the production rates. Measurements similar to Ref. [23] but specifically designed to check this energy extrapolation are warranted.

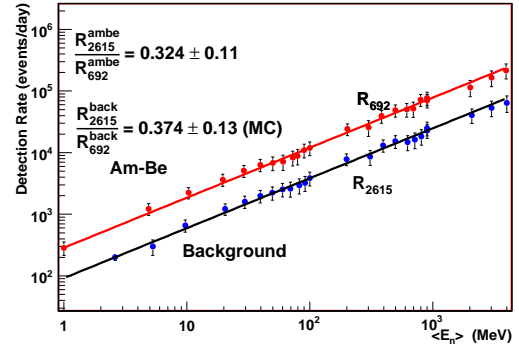


FIG. 6: The predicted production rates from the simulation of the  $^{208}\text{Pb}(n, n'\gamma)$  2614-keV and the  $^{72}\text{Ge}(n, n'\gamma)$  692-keV  $\gamma$  rays due to primary neutrons. The simulation is that of the CLOVER background-run geometry described in the text. Each data point represents a flux of mono-energetic neutrons impinging on the outside of the shield. The simulated flux was equal to the measured flux. The ratio is rather insensitive to incident neutron energy. The trend in energy is similar for other transitions. The vertical dashed lines indicate the average neutron energy for the two classes of neutrons.

##### B. The Special Cases of the 2023-keV, 2041-keV and 3062-keV $\gamma$ rays

The 2023-keV level in  $^{76}\text{Ge}$  can be excited by neutrons. The simulation predicts that this line is too weak to be seen in the CLOVER AmBe data, but the CLOVER is built of natural Ge. In the enriched detectors planned by future double-beta decay experiments, the fraction of isotope 76 is much larger and this line would be enhanced. Still our simulation (Table V) predicts it would be a very small peak.

The 3714-keV level in  $^{206}\text{Pb}$  can emit a 2041-keV  $\gamma$

ray. We only observed a candidate  $\gamma$ -ray peak in the coincidence data (Ge detector event in coincidence with a 4.4-MeV  $\gamma$  ray in the NaI detector) with the AmBe source radiating the Pb shield around the PopTop detector. The magnitude of this peak if it exists is small and not convincing. We use this data set to place a limit on the production rate of this line as it results in the most conservative limit.

In the AmBe-irradiated CLOVER and the non-coincidence PopTop spectra, we observed a 3062-keV  $\gamma$  ray that we assign to a transition from the 3633-keV level in  $^{207}\text{Pb}$ . (See Fig. 7.) This line is only present when Pb surrounds the detector: It is absent when Cu forms the shield. The statistical sensitivity was too weak in the PopTop coincidence spectrum to observe this weak line. In the CLOVER AmBe spectrum, the rate of this line is  $5.3 \times 10^{-3}$  that of 596-keV  $^{74}\text{Ge}$  peak rate and in the raw AmBe PopTop with Pb spectrum the ratio is  $4.5 \times 10^{-3}$ . From these data we can estimate an approximate rate that these dangerous backgrounds would be produced for a given neutron flux. In our surface laboratory, the CLOVER background rate for the  $^{74}\text{Ge}$  596-keV peak was 59.9 events/hr. This leads to a predicted rate of 0.3 events/hr in the 3062-keV peak. Note that our data indicate that any peak at 3062 keV is statistically weak ( $\leq 0.2$  events/hr) but reasonably consistent with this prediction. Note, in the AmBe-CLOVER runs, polyethylene blocks were used to increase the flux of thermal neutrons. It appears that these blocks contain some Cl and therefore we see indications of  $\text{Cl}(n,\gamma)$  lines. Even though  $^{35}\text{Cl}$  has a neutron capture line at 3062-keV, we do not assign the observed line in our data to that process. Because the  $^{35}\text{Cl}(n,\gamma)$  line at 2863 keV is not observed and because the line at 1959 keV is weak, we conclude that assigning this line to Cl would be inconsistent with the predicted line ratios for neutron capture. However, a concern regarding our assignment of the 3062-keV line to  $^{207}\text{Pb}$  is that one also expects a 2737-keV emission from the same 3633-keV level. This companion  $\gamma$  ray is not observed in our data and we plan future measurements dedicated to measuring the neutron-induced relative intensities of these two lines. If we assume that the entire rate (0.01 Hz) of the 3062-keV line is due to  $(n, n'\gamma)$ , we can make a crude estimate of the cross section by scaling to the rate in the 2614-keV line. The cross section for the 2614-keV  $(n, n'\gamma)$  is  $2.1 \text{ b} \pm 10\%$  [23]. Using this cross section, the relative rates in the two peaks, the different isotopic ratios of  $^{208}\text{Pb}$  and  $^{207}\text{Pb}$ , and the different  $\gamma$ -ray detection efficiencies, the average cross section for  $^{207}\text{Pb}(4.5\text{-MeV } n, n' \text{ 3062-keV } \gamma \text{ ray})$  is estimated to be 75 mb. The uncertainty is estimated to be about 20% or  $\sim 15$  mb.

From measurements with the CLOVER and a  $^{56}\text{Co}$  source, which has  $\gamma$ -ray energies near 3100 keV, we expect 0.13 DEP events per full-energy  $\gamma$ -ray event. Therefore, in our surface lab, we expect 0.03 events/hr in the DEP at 2039 keV due to  $^{207}\text{Pb}(n, n'\gamma)$ . This is well below our continuum rate of 2.5/keV-hr or 10/hr in an energy window corresponding to a 4-keV wide peak.

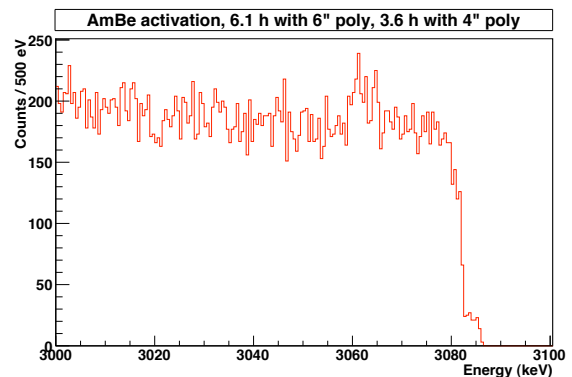


FIG. 7: The energy spectrum near 3000 keV showing the  $^{207}\text{Pb}(n, n'\gamma)$  3062-keV  $\gamma$ -ray line in the AmBe spectrum with the CLOVER.

Since our simulation does not predict all these lines, we summarize the measured rates normalized to the neutron flux in Table III to provide simple scaling to different experimental configurations. The uncertainties in Table III are estimates based on a minor contribution of the statistical uncertainty in the peak strengths and a major contribution resulting from the  $\approx 30\%$  uncertainty in the neutron flux determination as described in Section III B. Because the uncertainty is mostly systematic, there is a good possibility that the total uncertainties for each individual measurement are correlated. Therefore, to estimate the average values in this Table, we took a straight average of the individual values and then assigned an uncertainty equal to the largest fractional value. This procedure, although not rigorous, is more conservative than a weighted average. In addition, some peaks were not observed in all spectra. The upper limits on the strength of these peaks were estimated from the rates of weakest peaks observed near the associated energy region in the spectrum. Such peaks are considered to represent the level of sensitivity of our peak detection procedures. The 2041-keV line is a special case. We quote an upper limit based on the only spectrum that indicated a possible peak.

These measurements were done for a CLOVER detector inside a 10-cm Pb shield. The relative energy-dependent efficiency ( $\epsilon_{rel}$ ) for a full-energy peak in the CLOVER can be approximated by,

$$\epsilon_{rel} = 0.15 + 0.93e^{\frac{-(E_{\gamma}-148)}{766}}, \quad (5)$$

where  $E_{\gamma}$  is the  $\gamma$ -ray energy in keV. This expression is normalized to 1.0 at 209 keV and is estimated to have an accuracy of about 20% near 200 keV improving to about 10% at 2600 keV. The quoted relative efficiency for each of the 4 individual CLOVER detectors is 26% at 1.33 MeV as quoted by the manufacturer. Table III does *not* incorporate this efficiency correction, therefore the table presents the measured count rates with a minimum of assumptions. The thickness of Pb is large compared to

TABLE III: The raw count rates for select processes normalized to neutron flux of  $1/(cm^2y)$ . When extrapolating to neutron energies distant from that near the measurements, the uncertainty associated with the extrapolation must be included. See text for a discussion of the uncertainty estimates in this table especially with respect to the average.

Process	Rate	Rate	Rate	Rate
	AmBe-CLOVER	AmBe-PopTop ( $\frac{events}{ty}$ )	Background	Average
$^{206}Pb(n, n'537 - keV\gamma)$	$13.9 \pm 4.2$	$20.5 \pm 6.2$	$12.2 \pm 3.6$	$15.5 \pm 4.6$
$^{74}Ge(n, n'596 - keV\gamma)$	$164 \pm 49$	unresolved <sup>a</sup>	$142 \pm 43$	$153 \pm 46$
$^{207}Pb(n, n'898 - keV\gamma)$	$17.5 \pm 5.2$	$21.2 \pm 6.4$	$14.9 \pm 4.5$	$17.9 \pm 5.4$
$^{206}Pb(n, n'1705 - keV\gamma)$	$3.6 \pm 1.1$	$3.2 \pm 1.0$	$1.7 \pm 0.5$	$2.8 \pm 0.8$
$^{206}Pb(n, n'2041 - keV\gamma)$	$< 6.3$	$< 0.5$	$< 1.7$	$< 5.0^b$
$^{207}Pb(n, n'3062 - keV\gamma)$	$0.88 \pm 0.28$	$0.6 \pm 0.2$	$< 1.0$	$0.7 \pm 0.2$
<hr/>				
		( $\frac{events}{(keVty)}$ )		
Continuum Rate from $Pb, Ge(n, n'\gamma)$	$2.6 \pm 0.8$	$2.0 \pm 0.6$	$2.5 \pm 0.7$	$2.4 \pm 0.7$

<sup>a</sup>In the PopTop data, the 596-keV line was not resolved from nearby lines.

<sup>b</sup>The 2041 line was not observed in any of our spectra, however, a weak peak-like feature was present in the AmBe-PopTop coincidence data. We used the upper limit for the rate in that peak as the "average" as we considered this to be most conservative.

the mean free path of the  $\gamma$  rays of interest, therefore, the scaling should hold for other thick-shield configurations. Even so, the rates will be geometry-dependent so these results can only be considered guides when applied to other experimental designs. The rate of these excitations also depends on neutron energy. For the background run (AmBe run) the average neutron energy is  $\approx 6.5$  MeV ( $\approx 5.5$  MeV). Figure 6 shows that our simulations predict that the rate of these excitations scales as energy to the 0.81 power.

## V. DISCUSSION

### A. A Model of the CLOVER Background

We can use these experimental results to create a background model for our surface lab and then use simulation to extrapolate this model to better understand experiments done at depth. The measured rate for the continuum near 2039 keV was 14.8 events/(keV kg d). For the Th-wire data, this continuum rate was 0.10 events/(keV s) (2900 events/(keV kg d)) and for the AmBe data it was 0.09 events/(keV s) (2600 events/(keV kg d)). To determine the neutron-induced continuum rates in the AmBe data, however, we have to correct for the contribution due to two high-energy  $\gamma$  rays that are not part of the neutron-induced spectrum in the background. These are the  $\gamma$  rays from the 2223-keV  $p(n, \gamma)d$  and the 4.4-MeV  $\gamma$  rays originating from the  $(\alpha, n)$  reaction of the AmBe source itself. Although only  $\approx 10\%$  of these AmBe  $\gamma$  rays penetrate the 5-cm Pb shield, there is still a significant flux.

A simple simulation of the detector response to 2223-

keV  $\gamma$  rays can easily determine ratio of the rate in the 2039-keV region to that in the full-energy peak. Simulation indicates that this ratio is  $5.2 \times 10^{-2}$  /keV. Since the full-energy peak count rate is 5.813 Hz, we find this contribution to the continuum is 0.03 events/(keV s). For the 4.4-MeV  $\gamma$  ray from the source itself, simulation must determine an absolute rate in the continuum because the high-energy threshold prevented the observation of the full-energy peak or its escape peaks. The simulation predicts 0.03 events/(keV s). Subtracting these two contributions from the continuum rate for the AmBe source near 2039 keV results in a final value of 0.03 events/(keV s) or 860 events/(keV kg d).

Our background measurements were done without a cosmic ray anti-coincidence system. From auxiliary measurements with a scintillator in coincidence with the CLOVER and a similar shielding geometry, we measured the rate of  $\mu$  passing through the detector. In the continuum near the 2039-keV region, the rate is 5.4 events/(keV kg d).

From the Th-wire source data, we measure the ratio of the rate in the continuum near 2039 keV to that in the 2614 keV (16.3 Hz) peak to be  $6 \times 10^{-3}$ /keV. Of the 2614-keV peak rate in the background data,  $\approx 33\%$  is due to  $^{208}Tl$  decay. Scaling from the 2614-keV peak in the background data, the count rate near the 2039-keV region due to the Compton tail of the  $^{208}Tl$  2614-keV peak is 0.7 events/(keV kg d).

The remainder of the 2614-keV peak is due to neutron-induced processes. The contribution due to neutrons can be estimated from the AmBe data. For the AmBe data, the ratio of the rate in the continuum near the 2039-keV region (0.03 events(keV s)) to that for the 596-keV  $^{74}Ge(n, n'\gamma)$  peak (1.87 Hz) is  $1.6 \times 10^{-2}$ /keV. Scaling

TABLE IV: A summary of the count rate in the CLOVER background data in the energy region near 2039 keV based on the model deduced for the surface lab described in the text. The precision of the neutron-induced and muon-induced spectra simulations (Section II C and Ref [10]) is estimated to be about 30%. We take this to be a conservative estimate for the uncertainties associated with this Table.

Process	CLOVER Event Rate Surface Lab events/(keV kg d)
neutron-induced	8.3
$^{208}\text{Tl}$ Compton scattering	0.7
high energy $\mu$ continuum	5.4
Total from model	14.4
Measured Rate	14.8

from the  $^{74}\text{Ge}$  peak rate in the background data (59.9/h) indicates a rate of 7.8 events/(keV kg d) in the continuum near 2039 keV. That is, 53% of the events in that region are due to neutrons. One can do a similar scaling from the 692-keV  $^{72}\text{Ge}$  rates. Here the ratio is  $1.3 \times 10^{-2}/\text{keV}$  and the continuum rate is 8.8 events/(keV kg d). If we just scaled from the total 2614-keV peak using the scaling determined from the Th-wire source data, the continuum rate would be only 2.0 events/(keV kg d), clearly indicating that neutrons play a dominant role compared to  $^{208}\text{Tl}$  decay. The AmBe data can also be used to determine a scaling based on the 2614-keV line. The ratio is  $4.1 \times 10^{-2}/\text{keV}$ , much larger than for the Th-induced continuum. If we use this value and the estimate that 67% of the 2614-keV events are due to neutrons, we estimate a rate of 8.8 events/(keV kg d). We use the average of the Ge values as our estimate (8.3 events/(keV kg d) = 3000 events/(keV kg y)). Table IV summarizes the deduced contributions to the spectrum in the 2039-keV region.

## B. Solving the Problem with Overburden

The primary purpose of this study is to better understand the impact of neutrons on the background for future double-beta decay experiments. We explore this issue via two avenues. In this subsection, we use neutron fluxes from our simulations of the surface laboratory, measurements with the AmBe source, and simulations of the neutron flux in an underground laboratory to estimate the contribution of neutron-induced backgrounds underground. In the following subsection, we examine data from previous underground experiments.

The simulation of neutron processes in the 10-cm Pb shield and Ge comprising the CLOVER detector at the altitude of our laboratory predicts about 1393 events/(keV kg y) between 2000 and 2100 keV due to lead excitation and about 1167 events/(keV kg y) in this energy region due to germanium excitation. Our measured

value for the neutron-induced events is 3000 events/(keV kg y) to be compared with this predicted value of 2560 events/(keV kg y).

The simulation of the CLOVER within a 30-cm lead shield at a depth of 3200 mwe, predicts about 0.019 events/(keV kg y) contributed from lead excitation and about 0.016 events/(keV kg y) contributed from germanium excitation for a total of 0.035 events/(keV kg y). One can also just scale our surface-laboratory measurement of the neutron-induced rate near 2039 keV by the factor derived from Eqn. 4 above. This results in 0.05 events/(keV kg y). For a detector like the CLOVER, analysis based on pulse shape discrimination (PSD), and the response of individual segments or crystals can help reduce background based on its multiple-site energy deposit nature. These backgrounds can then be distinguished from the single-site energy deposit character of double-beta decay. We have measured the background reduction factor via these techniques to be  $\approx 5.9$  for the CLOVER [12].

Reference [10] provides a *quick reference* formula to estimate the neutron flux as a function of depth. The  $\mu$  flux and its associated activity is reduced by  $\approx 10$  for each 1500 m.w.e of added depth. Future double-beta decay experiments hope to reach backgrounds near 0.25 events/(keV t y). Our estimate of the rate at 3200 mwe is 35-50 events/(keV t y), which is a factor of 150 above the goal. Hence, greater depths would be desirable.

## C. Discussion of Previous Underground Experiments

Previous Ge-based double-beta decay experiments conducted deep underground [5, 6] set the standard for low levels of background. The future proposals however [8, 9] hope to build experiments with much lower backgrounds. In this subsection, we estimate how large the neutron contribution was to the previous efforts and future designs. Using the scaling summarized in Eqn. 4, we can compare the expectations of our simulated underground apparatus with previously published results. Table V shows this comparison. This table also presents a summary of how the rates would be affected by a change in depth only. The IGEX collaboration [5] has not published its data in sufficient detail to do a similar comparison. Other underground Ge detector experiments do not have the required sensitivity.

The Heidelberg-Moscow experiment [6] is a critical case study for such backgrounds and it was operated at a depth of 3200 mwe. One is clearly led to consider if the 3062-keV  $\gamma$  ray can explain the signal reported in Ref. [36, 37]. Figure 36 in Ref. [37], shows that no more than a few counts can be assigned to a 3062-keV  $\gamma$  ray. If the 23 counts assigned to double-beta decay were actually a DEP from this  $\gamma$  ray, the one would expect 175 counts or so in the 3062-keV peak. Therefore, it is difficult to explain the claimed peak by this mechanism. It is also

TABLE V: A summary of the key count rates arising from neutron interactions in the CLOVER background data in the energy region near 2039 keV as predicted by our analysis for three representative depths. The shield thickness is taken to be 30 cm and a veto system with an assumed efficiency of 90% is included. Except for the 2023-keV line, we used the scaling of Eqn. 4 to scale our CLOVER background measurements to the 3200 mwe depth and then used the muon fluxes at WIPP, Gran Sasso, and SNOLAB[10] to scale to the other depths. The Ge rates are also scaled for an enriched detector (86% isotope 76, 14% isotope 74). The scalings require the results from the simulations. The uncertainty from the scalings dominates and is estimated to be 30%. Since we did not observe the 2023-keV line, we used simulation to predict the rate. We used the measured upper limit for the 2041-keV line. For comparison, the results of Ref. [37] is shown. Reference [37] claims a result for zero-neutrino double-beta decay in an experiment performed at 3200 mwe. We entered the claimed event rate for that process in the same row as the 2041-keV line for comparison. The rate limits for the other lines assigned to Ref.[37] result from our estimates based on the figures in their papers and does not come directly from their papers.

Process	1600 mwe	3200 mwe	6000 mwe	Ref. [37]
$^{74}\text{Ge}$ 596 keV	19400/(t y)	1130/(t y)	15/(t y)	<800/(t y)
$^{76}\text{Ge}$ 2023 keV	30/(t y)	2/(t y)	0.02/(t y)	300/(t y)
$^{206}\text{Pb}$ 537 keV	4400/(t y)	250/(t y)	3.4/(t y)	
$^{207}\text{Pb}$ 898 keV	5300/(t y)	310/(t y)	4.2/(t y)	
$^{206}\text{Pb}$ 1705 keV	610/(t y)	36/(t y)	0.5/(t y)	
$^{206}\text{Pb}$ 2041 keV	<1300/(t y)	<74/(t y)	<1.0/(t y)	400/(t y)
$^{207}\text{Pb}$ 3062 keV	145/(t y)	8.4/(t y)	0.1/(t y)	<71/(t y)
continuum	880/(keV t y)	50/(keV t y)	0.7/(keV t y)	110/(keV t y)

clear that the predicted rate of the 2041-keV  $\gamma$  ray is too low to explain the data. The data from Ref. [37] show lines at 570 and 1064 keV. These lines were assigned to  $^{207}\text{Bi}$  present in the Cu. However, the spectra displayed in Fig. 13 of that paper shows that only detectors surrounded by Pb indicate the 570-keV line. Since there is no evidence for the 898-keV line in the data, we agree with the  $^{207}\text{Bi}$  assignment, however, we hypothesize that it must reside in the Pb and not the Cu. Perhaps this contamination is cosmogenically produced in Pb when it resides on the surface and not as a result of bomb testing as hypothesized by the authors[37].

Reference [37] also observed lines at 2011, 2017, 2022, and 2053 keV. These lines had rates of approximately 500/(t y), 500/(t y), 300/(t y) and 380/(t y) respectively. The line at 2022 keV is near a line we predict at 2023 keV. Reference [37] attributes these lines to weak transitions in  $^{214}\text{Bi}$ . From our analysis it is indicated that a negligible fraction of the peak at 2023 keV is neutron-induced. However, since the predicted strength of the tell-tale lines that would indicate a presence of neutron interactions is just below the sensitivity of that experiment, this conclusion is not without uncertainty. It has been pointed out that the strength in the 2022-keV line is too strong with respect to the  $^{214}\text{Bi}$  branching ratios even when summing uncertainties are taken into account [38, 39]. The analysis in Ref. [38], however, was based on a incorrectly normalized Fig. 1 in Ref [6]. A recent analysis [39] taking this into account still points to an inconsistency in the line strengths. This discrepancy could be resolved if one attributes a significant fraction of that peak to neutron interactions on  $^{76}\text{Ge}$ . Such an attribution is not supported by our simulations.

Reference [36] simulates the background in the Heidelberg-Moscow experiment resulting in a predicted

signal of  $646 \pm 93$  counts in the region between 2000 and 2100 keV during an exposure of 49.6 kg-y. This is a count rate of 130/(keV t y) to be compared with the quoted measured value for the data period simulated of 160/(keV t y). Their estimate indicates that only 0.2/(keV t y) are due to neutrons and they argue that  $\mu$ -generated neutrons are a negligible contribution. Our estimates indicate that neutrons are a more significant contribution and that the  $\mu$  contribution is significant. We are aware of no direct neutron flux measurements for neutrons above 25 MeV. The flux of neutrons with energy greater than 25 MeV is estimated in Ref. [36] to be  $10^{-11}/(\text{cm}^2 \text{ s})$  and they considered these neutrons to produce a negligible contribution to the background. In contrast, the simulation in Ref. [10] gives  $56 \times 10^{-11}/(\text{cm}^2 \text{ s})$  at 3200 m.w.e for the neutrons with energy greater than 25 MeV. We use this higher flux value and as a result, our estimate of the background rate near 2 MeV of 50/(keV t y) is comparable to the excess (30/(keV t y)) of the measured rate in comparison to the simulated rate in Ref. [36].

#### D. Is Copper an Alternative to Lead?

One has to consider the existence of a DEP line at the double-beta decay endpoint a serious design consideration for Ge-detector experiments. From the above analysis, the dangerous lines at 2041 and 3062 keV due to  $\text{Pb}(n, n'\gamma)$  are not significant contributors to the spectrum of Ref. [37]. However, as future efforts reduce the natural activity irradiating the detectors, these Pb-neutron interactions will become important. One solution could be the use of Cu as a shield instead of Pb. Copper is rather expensive and building the entire shield of this material is probably not necessary. A thick inner



liner of Cu might suffice, but if a peak is observed and Pb is present near the detector, arguments based on the spectrum near 3062 keV will be critical.

Although the problematic lines we observed in the Pb data were absent in our Cu data, the shields were too dissimilar to make a quantitative comparison regarding the effectiveness of reducing the continuum background. Furthermore, our experience with the lead and the simulation of  $(n, n'\gamma)$  spectra reduces confidence in the conclusion regarding the Cu in the absence of such data. We are preparing better experimental studies to address this question.

## VI. CONCLUSION

As double-beta decay experiments become more sensitive, the potential background must be constrained to ever-lower levels. Much progress has been made in reducing naturally-occurring radioactive isotopes from materials from which the detector is constructed. As these isotopes that have traditionally limited the experimental sensitivity are eliminated, rarer processes will become the dominant contributors. Here we have considered neutron-induced processes and have quantified them. Reactions involving neutrons can result in a wide variety of contributions to the background. That is, no single com-

ponent is likely to dominate. Therefore, tell-tale signatures for neutrons are needed and were identified in this work.

In addition to the general continuum background that neutrons might produce, two specific dangerous  $Pb(n, n'\gamma)$  lines were identified. These two backgrounds can be significantly reduced using depth and/or an inner layer of Cu within the shield. In particular, the 3062-keV transition in  $^{207}Pb$  has a double escape peak at the endpoint energy for double-beta decay in  $^{76}Ge$ . A comparison of past double-beta decay data indicates the rate of this transition is too small to explain a claim of double-beta decay.

## VII. ACKNOWLEDGMENT

We thank R.L. Brodzinski for discussions regarding the historical production of  $^{207}Bi$  and its possible presence in the environment. We thank John Wilkerson and Jason Detwiler for useful suggestions and discussion. Finally, we also thank Alan Poon and Werner Tornow for useful discussions and a careful reading of the manuscript. This work was supported in part by Laboratory Directed Research and Development at Los Alamos National Laboratory.

- 
- [1] Steve R. Elliott and Petr Vogel, *Annu. Rev. Nucl. Part. Sci.* **115** (2002)
  - [2] Steven R. Elliott and Jonathan Engel, *J. Phys. G: Nucl. Part. Phys.* **30**, R183 (2004).
  - [3] F.T. Avignone III, G.S. King III and Yuri Zdesenko, *New Journal of Physics* (in press 2004).
  - [4] A.S. Barabash, *Physics of Atomic Nuclei*, **67**, No. 3, 438 (2004).
  - [5] C.E. Aalseth, *et al.*, *Phys. Rev. C* **59**, 2108 (1999).
  - [6] H.V. Klapdor-Kleingrothaus, *et al.*, *Eur. Phys. J* **A12**, 147 (2001);
  - [7] H.V. Klapdor-Kleingrothaus, *et al.*, *Nucl. Instr. and Meth.* **A522**, 371(2004).
  - [8] R. Gaitskell, *et al.*, *nucl-ex/0311013* (2003).
  - [9] I. Abt, *et al.*, "A New  $^{76}Ge$  Double Beta Decay Experiment at LNGS", *hep-ex/0404039* (2004).
  - [10] D.-M. Mei and A.Hime, *Phys. Rev.* **D73** 053004 (2006).
  - [11] The CLOVER detector is manufactured by Canberra Eurysis, 800 Research Parkway, Meriden CT 06450, USA.
  - [12] S. R. Elliott, *et al.*, *Nucl. Instr. and Meth.* **A558** 504 (2006).
  - [13] The PopTop detector is manufactured by ORTEC, 801 South Illinois Avenue, Oak Ridge, TN 37830.
  - [14] X-Ray Instruments Associates, 8450 Central Ave., Newark CA 94560, USA.
  - [15] Wavemetrics Inc., PO Box 2088, Lake Oswego, OR 97035, USA.
  - [16] Rene Brun and Fons Rademakers, *Nucl. Instr. and Meth.* **389**, 81 (1997); <http://root.cern.ch>
  - [17] *Table of Isotopes*, Eds. Richard B. Firestone and Virginia S. Shirley, John Wiley and Sons, Inc., New York (1996).
  - [18] R.Brun, *et al.*, "GEANT3", CERN DD/EE/84-1 (revised), 1987.
  - [19] C.Zeitnitz, *et al.*, *Nucl. Instr. and Meth. in Phys. Res.* **A349**, 106 (1994).
  - [20] W. Hauser and H. Feshbach, *Phys. Rev.* **87**, 366 (1952).
  - [21] P. A. Moldauer, *Phys. Rev.* **123**, 968 (1961).
  - [22] Richard M. Lindstrom, *et al.*, *Nucl. Instr. and Meth.* **A299**, 425 (1990).
  - [23] H. Vonach, *et al.*, *Phys. Rev. C* **50** (1994) 1952.
  - [24] A. Pavlik, *et al.*, *Phys. Rev. C* **57**, 2416 (1998).
  - [25] The National Nuclear Data Center, Brookhaven National Laboratory, Upton, New York, 11973-5000.
  - [26] K.C. Chung, *et al.*, *Phys. Rev. C* **2**, 139 (1970).
  - [27] R.L. Bunting and J.J. Kraushaar, *Nucl. Instrum. Meth.* **118**, 565 (1974).
  - [28] Richard M. Lindstrom, *et al.*, *Nucl. Instrum. Meth.* **A299**, 425 (1990).
  - [29] G. Fehrenbacher, R. Meckbach, and H.G. Paretzke, *Nucl. Instrum. Meth.* **A372**, 239 (1996).
  - [30] G.P. Škoro, *et al.*, *Nucl. Instrum. Meth.* **A316**, 333 (1992).
  - [31] P.H. Stelson, *et al.* *Nucl. Instr. and Meth.* **A98**, 481 (1972).
  - [32] R. Wordel, *et al.*, *Nucl. Instr. and Meth.* **A369**, 557 (1996).
  - [33] J.F. Ziegler, *IBM J. Res. Develop.* **40**, 19 (1996).
  - [34] J.F. Ziegler, *IBM J. Res. Develop.* **42**, 117 (1998).
  - [35] P. Goldhagen, *et al.*, *Nucl. Instr. and Meth.* **A476**, 42 (2002).



- [36] C. Dörr, H.V. Klapdor-Kleingrothaus, Nucl. Instr. and Meth. **A513**, 596 (2003).
- [37] H.V. Klapdor-Kleingrothaus, A. Dietz, I.V. Krivosheina, and O. Chkvorets, Nucl. Instr. and Meth. **A522**, 371 (2004).
- [38] C.E. Aalseth, *et al.*, Mod. Phys. Lett. **A17**, 1475 (2002).
- [39] R. L. Brodzinski, “Regarding the Over-Estimation of the Intensity of the Minor Photopeaks of  $^{214}\text{Bi}$  in the Heidelberg-Moscow Experiment,” PNNL-SA-49010 (2006).